Magnetic Field Amplification in Mechanically Driven Compressible Magnetohydrodynamic Turbulence

John V. Shebalin*
NASA Langley Research Center, Hampton, Virginia 23665
and
David Montgomery†
Dartmouth College, Hanover, New Hampshire 03755

Magnetic field amplification in a homogeneous, dissipative, isentropic, polytropic, two-dimensional, turbulent magnetofluid is simulated numerically. The magnetofluid is, in a number of cases, mechanically forced so that energy input balances dissipation and thereby maintains a steady state. In the presence of a spatially-uniform mean magnetic field, a magnetofluid whose initial turbulent magnetic energy is zero quickly arrives at a state of nonzero turbulent magnetic energy. If the mean magnetic field energy density is small, the turbulent magnetic field can achieve a local energy density more than 400 times larger than the energy density associated with the mean magnetic field; if the mean magnetic field energy density is large, then equipartition between the turbulent magnetic and kinetic energy is achieved at the smaller scales. Compared to the presence of a mean magnetic field, compressibility appears to have only a marginal effect in mediating the transfer of turbulent kinetic energy into magnetic energy.

Introduction

COMPRESSIBLE, ionized, turbulent flow occurs in many contexts. These include magnetic and inertial fusion energy devices, astrophysical objects, and the ionosphere. Another context is the environment around aerospace vehicles which operate in hypersonic regimes (such as reentering spacecraft). In all these cases, magnetohydrodynamic (MHD) and other plasma effects may become significant or at least observable. In many of these cases, there is an externally imposed mean magnetic field present (such as the Earth's magnetic field). A mean magnetic field is important in that it may lead to flow states where an appreciable amount of the local energy density is invested in the self-excited turbulent magnetic field, even though there was negligible initial self field (i. e., the magnetic field associated with current densities locally present in the magnetofluid).

The energy contained in the self-excited turbulent magnetic field may, in fact, become several orders of magnitude larger than the relatively small amount of energy contained in the local mean magnetic field. A *magnetic amplification* process has obvious importance in explaining many natural phenomena; it has also been observed in numerical simulations of *decaying* homogeneous turbulence.[1] Since turbulent MHD flow in many contexts is *driven,* rather than merely decaying, it is important to determine the response of a compressible turbulent magnetofluid to the presence of both external forcing and a mean magnetic field. It is this situation that we have numerically simulated and that we wish to present here.

Some ramifications of such a study lie in the possible effects a relatively large turbulent magnetic field may have, for example, on heating rates and body forces. On the other hand, even if the magnetic energy is small compared to the fluid kinetic energy, the presence of an observable turbulent magnetic field may provide a means for determining fluid fluctuation levels: since these are correlated with magnetic fluctuations, the use of a magnetometer might provide useful information concerning both.

Although it would be preferable to examine directly bounded, geometry-specific, three-dimensional flows, doing so with good spatial resolution requires computers considerably more "super" than currently exist—particularly if we wish to investigate a large number of parameter values in an efficient manner. This along with a dearth of fundamental results dictates that we first investigate *homogeneous* MHD turbulence, i.e., turbulence that, though initiated by boundary effects, is far enough away from that boundary that it behaves as if it were a small volume of turbulent fluid embedded in a larger, homogeneous volume. (If the assumption of spatial homogeneity is made, then an efficient numerical procedure for simulating MHD turbulence is a Fourier spectral transform method.[2,3])

Furthermore, in order to maintain good spatial resolution, two-dimensional simulations are more efficacious than three dimensional (due to practical limitations on computer memory and speed) as long as the important physical phenomena that exist in three dimensions are still retained in the two-dimensional model. This is a severe restriction with regard to what have come to be called "dynamo" processes if our model magnetofluid is not embedded in a mean magnetic field, since various two-dimensional "anti-dynamo" theorems recognize that there can be no turbulent magnetic field enhancement in this case.[4] However, a nonzero mean field provides an effective coupling in two dimensions, as well as three dimensions between turbulent kinetic and magnetic energy. Although three-dimensional MHD may be expected to hold many more interesting phenomena than two-dimensional MHD, the effect of a mean magnetic field should be similar in both; thus, we proceed on our path of numerically exploring two-dimensional magnetofluids with the expectation that mean field effects will be at least qualitatively similar in two and three dimensions. Since a small but nonzero mean magnetic field may be present in many cases, and since its presence causes the antidynamo theorem to fail, the physical significance of this theorem may be less, for two-dimensional flows, than it has sometimes been made to appear.

Received April 1989; revision received July 1989.

*Aero-Space Technologist. Member AIAA.
†Professor, Department of Physics and Astronomy.

Following a description of the basic equations, a numerical procedure for simulating a two-dimensional homogeneous, isentropic, polytropic magnetofluid will be discussed. Numerical results will then be given and followed by a discussion and conclusion.

Fundamental Equations

The basic, nondimensional three-dimensional single fluid MHD equations are

$$\frac{\partial \rho}{\partial t} + \nabla \cdot \rho \boldsymbol{u} = 0 \tag{1a}$$

$$\rho\left(\frac{\partial \boldsymbol{u}}{\partial t} + \boldsymbol{u} \cdot \nabla \boldsymbol{u}\right) = -\beta \nabla p + \boldsymbol{j} \times (\boldsymbol{B}_0 + \boldsymbol{b}) + \rho \boldsymbol{g} + \boldsymbol{F} + \nabla \cdot \left[\mu \nabla \boldsymbol{u} + \left(\frac{\mu}{3} + \zeta\right) \boldsymbol{I} \nabla \cdot \boldsymbol{u}\right] \tag{1b}$$

$$\frac{\partial \boldsymbol{b}}{\partial t} = \nabla \times [\boldsymbol{u} \times (\boldsymbol{B}_0 + \boldsymbol{b}) - \eta \boldsymbol{j} + \boldsymbol{G}]$$

$$\boldsymbol{b} = \nabla \times \boldsymbol{a}, \qquad \boldsymbol{j} = \nabla \times \boldsymbol{b} \tag{1c}$$

$$\frac{\partial T}{\partial t} + \boldsymbol{u} \cdot \nabla T = (1 - \gamma) T \nabla \cdot \boldsymbol{u} + \frac{1}{\rho} \nabla \cdot \left(\frac{\kappa}{c_p} \nabla T\right) + \frac{\gamma - 1}{\beta \rho}\left\{\frac{\mu}{2} \tau_{ij} \tau_{ij} + \eta j^2 + \zeta (\nabla \cdot \boldsymbol{u})^2 + H\right\}$$

$$(\tau_{ij} = \partial_i u_j + \partial_j u_i - \frac{2}{3} \delta_{ij} \nabla \cdot \boldsymbol{u}) \tag{1d}$$

The velocity $\boldsymbol{u}$ and magnetic field $\boldsymbol{B}$ are measured in terms of reference values U_0 and B_0, respectively, and the reference values for length, temperature, and time are L_0, T_0 and t_0, respectively, ($t_0 \equiv L_0/U_0$). The magnetic field consists of two parts, $\boldsymbol{B} = \boldsymbol{B}_0 + \boldsymbol{b}$, i.e., an externally produced mean part $\boldsymbol{B}_0$ and the internal, self-consistently determined part $\boldsymbol{b}$. In Eq. (1), $\boldsymbol{F}$, $\boldsymbol{G}$, and H are forcing terms used to model the injection of turbulent excitations; e.g., these may be due to thermal instabilities upstream in a shock transition layer, a situation that occurs in laser-produced plasmas,[5] and which may be expected in re-entry vehicle plasma sheaths. [The $\boldsymbol{F}$, $\boldsymbol{G}$, and H are not generally imposable independently of each other or of any approximations which may also be imposed on the set of Eqs. (1).] The local gravitational acceleration is $\boldsymbol{g} = -\nabla \Phi$ (Φ is the static gravitational potential), and other quantities and their (units) are

ρ : mass density (ρ_0)
p $= \rho T$: pressure ($\rho_0 T_0$)
γ $\equiv (c_p/c_v)$: ratio of specific heats
c_p : specific heat at constant pressure (U_0^2/T_0)
c_v : specific heat at constant volume (U_0^2/T_0)
μ : viscosity ($\rho_0 U_0 L_0$)
ζ : bulk viscosity ($\rho_0 U_0 L_0$)
η : electrical resistivity ($U_0 L_0$)
κ : thermal conductivity ($\rho_0 U_0^3 L_0/T_0$)
β $\equiv (p_0/\rho_0 U_0^2)$: a measure of compressibility
$\boldsymbol{I}$ $\equiv \Sigma_{i=1}^{3} \hat{\boldsymbol{e}}_i \otimes \hat{\boldsymbol{e}}_i$: unit 2nd rank tensor

In those situations when the magnetic energy is comparatively small, U_0 may be an rms fluid velocity $U_0 = \sqrt{[u^2]}$, and in the case where the magnetic energy is comparatively large, $U_0 = V_A \equiv B_0/\sqrt{4\pi\rho_0}$ (cgs units); B_0 is either the mean-field strength or the rms value of $\boldsymbol{b}$, and V_A is the *Alfven velocity*. If the magnetic and kinetic energies are comparable, $V_A \approx \sqrt{[u^2]}$ and U_0 can represent either one.

The energies we are concerned with here are

E_K $= E_s + E_c$: total kinetic energy
E_s $= [p_s \cdot u_s/2]$: *solenoidal* part of E_K
E_c $= [p_c \cdot u_c/2]$: *compressional* part of E_K
E_B $= [\boldsymbol{b} \cdot \boldsymbol{b}/2]$: magnetic energy
E_I $= [\beta/(\gamma - 1)\rho(T - T_0)]$: net internal energy
E_g $= [\rho\Phi]$: gravitational energy
E_{com} $= E_c + E_I$: total compressional energy
E $= E_s + E_B + E_{\text{com}} + E_g$: total energy

and four other important quantities are

Ω $\equiv [(\nabla \times \boldsymbol{u})^2]$: enstrophy
J $\equiv [(\nabla \times \boldsymbol{b})^2]$: mean squared current
A $\equiv [\rho a^2]$: mean squared vector potential
H_c $\equiv [\boldsymbol{u} \cdot \boldsymbol{b}]$: "cross helicity"

(The square brackets signify a volume average over the computational box:

$$[Q] \equiv \frac{1}{(2\pi)^2} \int_0^{2\pi} dx \int_0^{2\pi} dy\, Q(x,y)$$

and the solenoidal and compressible parts of the momentum density are defined as $\boldsymbol{p}_s \equiv \rho \boldsymbol{u}_s$ and $\boldsymbol{p}_c \equiv \rho \boldsymbol{u}_c$, respectively.)

Furthermore, the dynamical system described by Eqs. (1) has the conservation law:

$$\frac{dE}{dt} = [\boldsymbol{u} \cdot \boldsymbol{F} + \boldsymbol{j} \cdot \boldsymbol{G} + H] \tag{2a}$$

Note that E is theoretically conserved if $\boldsymbol{F} = \boldsymbol{G} = 0$, $H = 0$, even if the dissipation coefficients μ, ζ and η are nonzero (for the full set of equations).

The fundamental equations are very general and can be applied to study any number of physical situations (e.g., magneto-aerodynamics, geophysics, many astrophysical situations, and plasma confinement devices). Depending upon the application, the transport coefficients μ, ζ, η, and κ may be constant or may vary with temperature, density, or magnetic field strength.

In our work here, we will not solve the full set of Eqs. (1), but instead will simplify them by making the following three assumptions: first, we assume an isentropic, polytropic equation of state $p = \rho T = \rho^\gamma$ so that $T = \rho^{\gamma - 1}$. Second, we set $G = 0$ and $\zeta = \kappa = 0$; concurrently and in order that Eq. (1d) be identically satisfied (and need no longer be explicitly considered), we must choose H to be a "heat sink":

$$H = -\left[\frac{\mu}{2} \tau_{ij} \tau_{ij} + \eta j^2\right]$$

All of this modifies Eq. (2a), so that we have

$$\frac{dE}{dt} = \left[\boldsymbol{u} \cdot \boldsymbol{F} - \frac{\mu}{2} \tau_{ij} \tau_{ij} - \eta j^2\right] \tag{2b}$$

If $F = 0$ and $\mu = \eta = 0$, E is an "integral invariant" of the compressible flow. If there is still no forcing ($F = 0$) but dissipation exists ($\mu \neq 0$ and/or $\eta \neq 0$), the energy E can only decrease. Finally, if we wish to maintain a "steady state" in the presence of dissipation, we can determine F (numerically at each time step) so that the right side of Eq. (2b) is zero.

Third, the basic parts of Eqs. (1) are further reduced by restricting dynamics to two dimensions (here, the x-y plane). In this case, Eq. (1c) can be "uncurled" to yield

$$\frac{\partial a}{\partial t} = \boldsymbol{u} \times (\boldsymbol{B}_0 + \boldsymbol{b}) - \eta \boldsymbol{j} \tag{3}$$

where

$$a = a\,(x,y,t)\hat{\boldsymbol{e}}_z, \qquad \boldsymbol{b} = -\hat{\boldsymbol{e}}_z \times \nabla a, \qquad \boldsymbol{j} = -\nabla^2 a$$

$$\boldsymbol{u} = \boldsymbol{u}\,(x,y,t), \qquad \boldsymbol{u} \cdot \hat{\boldsymbol{e}}_z = 0, \qquad \boldsymbol{B}_0 = B_0 \hat{\boldsymbol{e}}_x$$

Note that there is no gradient in Eq. (3) due to the uncurling: any gradient is in the x-y plane, and Eq. (3) has no component in that plane. (If $\boldsymbol{B}_0$ had been given a component out of the x-y plane, a different description would have resulted.)

Now, if we take a scalar product of Eq. (3) with ρa, add this to the product of Eq. (1a) with $a^2/2$, and volume average, the result (after some manipulation) is

$$\frac{1}{2}\frac{dA}{dt} = \boldsymbol{B}_0 \cdot [\rho \boldsymbol{a} \times \boldsymbol{u}] - \eta[\rho b^2 - \frac{1}{2} a^2 \nabla^2 \rho] \tag{4}$$

where, again, $A \equiv [\rho a^2]$. Thus, if $\eta = 0$ and $B_0 = 0$ in two dimensions, A is an integral invariant for inviscid, compressible MHD; magnetic energy is effectively restricted from growing, and we have a variant of the familiar anti-dynamo theorem. However; if $\eta = 0$ but $B_0 \neq 0$, A can grow through a mean-field effect; also, if $\eta \neq 0$, A gains a possible "resistive source" in which compressional energy can cause A (and other magnetic quantities) to grow. (In the numerical work that follows, it will be seen that the mean-field effect can be important, whereas the resistive source of A produces a negligible effect.)

In the following sections, we model a two-dimensional magnetofluid using Eqs. (1a) and (1b) with $\boldsymbol{g} = 0$, and Eq. (3) along with the four assumptions listed above. The magnetofluid is mechanically forced (but not magnetically forced), and the mean magnetic field strength is varied (along with the initial Mach number). It should be noted that the isentropic, polytropic approximation is a considerable simplification of the problem involving a temperature equation.

Computational Procedure

The numerical procedure we use is based on the dealiased spectral transform method of Patterson and Orszag.[2,3] which we have used to good advantage previously (e.g., in Ref. 6). In addition, we use the natural logarithm of the density (and, in the future, the temperature) rather than the density (or temperature) directly as a computational variable:

$$\lambda = \ell n \rho \qquad \vartheta = \ell n T$$

This ensures that any numerical time-integration scheme will not produce negative values of density or temperature. [In the isentropic polytropic case, $\vartheta = (\gamma - 1)\lambda$.]

In the numerical procedure, the dynamical fields are expanded in Fourier series

$$\begin{aligned}
\lambda(x,t) &= \sum_{|k| \leq K_{\max}} \lambda(k,t) e^{-ik \cdot x} \\
\boldsymbol{u}(x,t) &= \sum_{|k| \leq K_{\max}} \boldsymbol{u}(k,t) e^{-ik \cdot x} \\
\boldsymbol{b}(x,t) &= \sum_{|k| \leq K_{\max}} \boldsymbol{b}(k,t) e^{-ik \cdot x} \\
\vartheta(x,t) &= \sum_{|k| \leq K_{\max}} \vartheta(k,t) e^{-ik \cdot x}
\end{aligned} \tag{5}$$

In the case of three-dimensional simulations, the position vector is $\boldsymbol{x} = (x,y,z)$, and the wave vector is $\boldsymbol{k} = (k_x,k_y,k_z)$; here, for two-dimensional simulations, the position vector is $\boldsymbol{x} = (x,y)$, and the wave vector is $\boldsymbol{k} = (k_x,k_y)$; $K_{\max}$ is the maximum modulus of $\boldsymbol{k}$. Here, Eqs. (5) are placed in the basic parts of Eqs. (1a), (1b), and (3) to yield a set of many hundred or thousand ordinary, coupled differential equations. Time integration is performed by a second-order Runge-Kutta method with the dissipative terms being evaluated as implicitly as possible.

Aliasing can be avoided in the formation of high-order products in terms such as

$$\rho,\ \rho^{\gamma},\ \rho^{-1},\ T,\ \rho T,\ (\rho T)^{-1}$$

through the use of expansions such as

$$\rho^{\alpha} = e^{\alpha\lambda} = 1 + \alpha\lambda + \left(\alpha\lambda, \frac{\alpha\lambda}{2}\right) + \left[\left(\alpha\lambda, \frac{\alpha\lambda}{2}\right), \frac{\alpha\lambda}{3}\right] + \ldots \tag{6}$$

The nth term in the series is a fully dealiased quadratic product formed from the preceding term and $\alpha\lambda/n$, and summation continues until machine accuracy is reached. The curly brackets $\{a,b\}$ signify that a single, dealiased quantity has been formed from a and b by the Patterson-Orszag transform method.[3] Although this fully spectral procedure avoids aliasing, its benefits are often outweighed by the increase in computational time; transforming to x-space, forming $e^{\alpha\lambda}$ directly, and then transforming back to k-space cuts down the computational time per time step by a factor of 2–4. If we maintain the Patterson-Orszag dealiasing procedure everywhere except for the calculation of $\rho(\boldsymbol{k})$ and its powers, we have a method for compressible flows.

Furthermore, the arrays which contain dynamic variables, their derivatives, and products are minimal arrays, rather than full fast Fourier transform (FFT) arrays (of which there are only two in the code). In a Patterson-Orszag dealiasing method,[3] the FFT arrays are somewhat sparse, a two-dimensional array containing 30% zeros and a three-dimensional array containing 56% zeros. The minimal array consists of only the nonzero FFT array elements; mapping to and from the FFT arrays is accomplished by a bit vector or order array. Mapping into the minimal array also serves the purpose of isotropic truncation, as required by the Patterson-Orszag method.[3]

Finally, steady-state forcing is accomplished in the following manner: the forcing term $\boldsymbol{F}$ in Eq. (1b) is defined at each time step by $\boldsymbol{F}(\boldsymbol{k}) = \alpha \boldsymbol{f}(\boldsymbol{k})$, where

$$f(k) = f(k)\ [\cos\theta(k)\ e^{i\varphi_x(k)}\hat{\boldsymbol{e}}_x + \sin\theta(k) e^{i\varphi_y(k)}\hat{\boldsymbol{e}}_y] \tag{7}$$

The phase functions

$$\theta(k),\ \varphi_x(k),\ \text{and}\ \varphi_y(k)$$

have random initial values between $-\pi$ and π and are incremented at each time step for each k by the prescription

$$\theta(k) + 2\pi \cdot \delta \cdot (f - 0.5) \rightarrow \theta(k)$$

$$\varphi_x(k) + 2\pi \cdot \delta \cdot (f - 0.5) \rightarrow \varphi_x(k)$$

$$\varphi_y(k) + 2\pi \cdot \delta \cdot (f - 0.5) \rightarrow \varphi_y(k)$$

where f is a generating function that yields a random number between 0 and 1 every time it is called and δ typically has a value of 0.01 to 0.03. Note that the injected kinetic energy is half compressional and half solenoidal when averaged over time or over k.

Since time step size generally varies during a simulation of compressible turbulence, so does the effective correlation time of our random forcing (since δ is held constant). However, the exact value of δ did not appear to be very important. In fact, in some preliminary runs, it was found that setting $\delta = 0$ did not noticeably change the qualitative nature of a run. We have not fully explored the effects of varying δ (or of redefining it so that $\delta\Delta t$ = constant), but we do not expect the exact details of forcing at the large scales to be "remembered" during the turbulent transfer of energy to the small scales of the flow.

The spectral magnitude function $f(k)$ in Eq. (7) has the form

$$f(k) = \exp[-(k - k_0)^2/2\sigma^2] \tag{8}$$

When forcing is turned "on" (as well as dissipation), the initial value of total energy E is saved, and after each time step, the energy is reset to the initial value by choosing α

properly: since, after each dynamical iteration, E has decreased by $\Delta E(=H\Delta t)$ from the initial value, the parameter α is determined by Eq. (2b):

$$\alpha = \frac{-\Delta E/\Delta t}{[u \cdot f]}$$

Note that energy is replaced at a prescribed part of the mechanical (kinetic) energy spectrum whereas it is lost through dissipation (viscosity and resistivity)—presumably more so at high k.

We have used this (fully spectral, unforced) algorithm to study numerically[6] theoretical predictions made earlier by Montgomery et al.[7] to explain the observed spectral structure of small amplitude turbulent density fluctuations in the interstellar medium.[8] The theoretical predictions made by Montgomery et al.[7] followed from the assumption that interstellar density fluctuations were inherently related to the magnetohydrodynamics rather than just the hydrodynamics[9] of the interstellar medium. The prediction was, in effect, that the total pressure (magnetic plus thermodynamic) was essentially constant at the smaller spatial scales. Assuming (among other things) that the statistical behavior of both kinetic and magnetic omnidirectional energy spectra was described by $k^{-5/3}$ led to the conclusion that the omnidirectional density fluctuation spectrum behaved as $k^{-5/3}$, which agreed with several astrophysical observations[8] spanning 12 spatial orders of magnitude; in contrast, a long-standing, purely hydrodynamic argument led to a predicted $k^{-7/3}$ behavior. The numerical work of Ref. 6 verified, in turn, that the theory also matched data generated by direct numerical simulation, even when the Reynolds numbers are not large enough to expect inertial range power laws.

Numerical Results

In the two-dimensional simulations presented here, the transport coefficient η is assumed constant and $\kappa = \zeta = 0$ in Eq. (1), and the viscosity μ is linearly related to the density. This form of μ is a great simplification of what is expected for "low-temperature" plasmas[10] or fully ionized plasmas.[11] (If this form of the viscosity is heuristically adopted in the Navier-Stokes (NS) case also, it removes the constraint imposed by density fluctuations that limited the time step of the NS runs of Passot and Pouquet.[12] In the MHD case, however, the presence of the magnetic force term requires that this constraint be retained whenever the magnetic force is locally large.)

The computations were done on a 64×64 grid, a size chosen so as to allow for a sufficient number of runs at different parameter values. The runs consist of six fully spectral ones (1–6) and four semispectral ones (7–10). The initial spectra for these runs are shown in Fig 7; furthermore, $[u^2] = 1$ at $t = 0$; therefore the initial Mach numbers corresponding to each run are given by $Ma = c_s^{-1} = (\beta\gamma)^{-1/2}$, where c_s is the sound speed. In all runs, there was no initial turbulent magnetic field energy, but there was a mean magnetic field $\boldsymbol{B}_0 = B_0\hat{\boldsymbol{e}}_x$ present. Those runs that were driven all had $k_0 = 10$ and $\sigma = 4$ in Eq. (8). Parameters for all the runs are given in Table 1.

The dissipation wave numbers for these runs were 25–35 (in Eq. (5), $K_{\max} = 30.2$). The viscous microscale Reynolds numbers were close to 20 for $B_0 = 0.5$ and close to 45 for $B_0 = 0.001$ The microscale magnetic Lundquist numbers were close to 0 for $B_0 = 0.001$ and close to 40 for $B_0 = 0.5$.

There are two time scales in the compressible systems studied here. There is the "eddy-turnover-time" scale, which is characterized by $t_\epsilon \approx L_0/U_0$[13]; this is the same as our previously defined characteristic time t_0. There is also a "sound-wave-transit-time" $\tau_0 = c_s t_0/U_0 = t_0/Ma$; in the definition of τ_0 the initial values of Ma and $U_0(=1)$ are used. Thus, either t (in units of t_0) or τ (in units of τ_0) can be used; although we have expressed our graphical results here in terms of τ.

Eddy turnover times can be more precisely defined as

$$t_\epsilon = \frac{2\pi}{\omega_{\text{ave}}}$$

where

$$\omega_{\text{ave}}^2 = \frac{1}{t_f}\int_0^{t_f} \Omega \mathrm{d}t$$

and Ω is the enstrophy. Here, for the dissipative runs 3–6, the average is $t_\epsilon = 0.95$ ($\tau_\epsilon = 2.8$) and for run 10, $t_\epsilon = 0.80$ ($\tau_\epsilon = 0.96$).

Discussion

In Fig. 1 the various volume averaged (global) quantities which were previously defined are shown for run 1; in this run there was no forcing or dissipation, and the apparent energy conservation is a property of the spectral method. The total energy appears to be a "rugged invariant"; although this cannot be analytically proven for a truncated Fourier representation of a compressible magnetofluid system as it can for an incompressible one.[14]

In Fig. 2 we have run 2 in which the dissipation is turned on, but forcing is not; the resulting behavior is as expected from previous experience. In Fig. 3 we have run 3, which has the same initial conditions as runs 1 and 2 but with both the dissipation and forcing turned on. Runs 1, 2, and 3 all have a relatively large mean magnetic field (0.5), which appears to cause an appreciable amount of magnetic field amplification.

Runs 1, 2, and 3 are all fully spectral; in order to have confidence in the semispectral method, a simulation corresponding to run 1 was performed, but the semispectral varia-

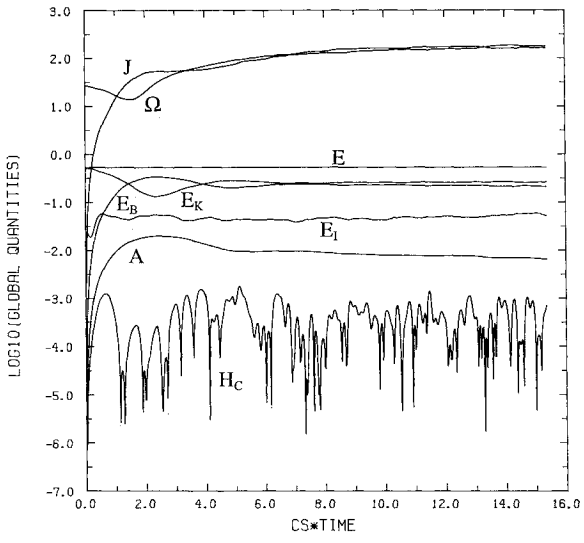

Fig. 1 Run 1: fully spectral, unforced, $\nu = \eta = 0$, $\beta = 6$, $\gamma = 1.5$, $B_0 = 0.5$.

Table 1 Run parameters

Run	β	γ	B_0	ν,η	F/S[a]	Δt's	Force	τ_{final}[b]
1	6	1.5	.50	.00	F	7500	off	15.4
2	6	1.5	.50	.01	F	5500	off	12.4
3	6	1.5	.50	.01	F	4500	on	8.6
4	6	1.5	.20	.01	F	7000	on	12.3
5	6	1.5	.05	.01	F	9000	on	14.6
6	6	1.5	.001	.01	F	5500	on	21.1
7	6	1.5	.50	.00	S	7500	off	15.8
8	1	1.44	.001	.00	F	2000	off	0.89
9	1	1.44	.001	.00	S	500	off	0.88
10	1	1.44	.001	.01	S	18,000	on	15.4

[a]F: fully spectral, S: semispectral. [b]Final time in units of τ_0.

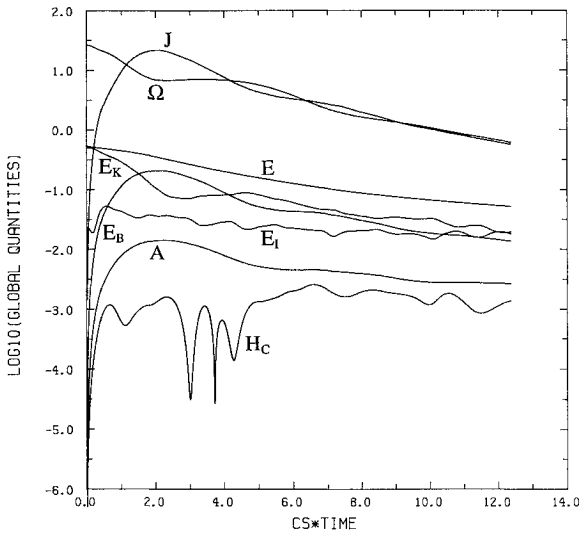

Fig. 2 Run 2: fully spectral, unforced, $\nu = \eta = 0.01$, $\beta = 6$, $\gamma = 1.5$, $B_0 = 0.5$.

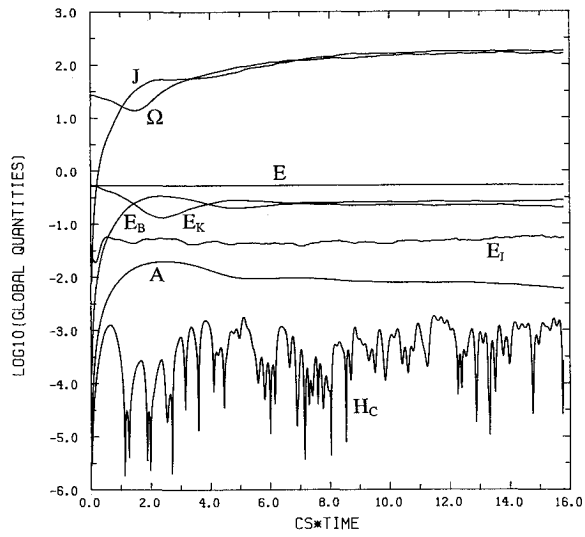

Fig. 4 Run 7: semispectral, unforced, $\nu = \eta = 0$, $\beta = 6$, $\gamma = 1.5$, $B_0 = 0.5$ (see Fig. 1).

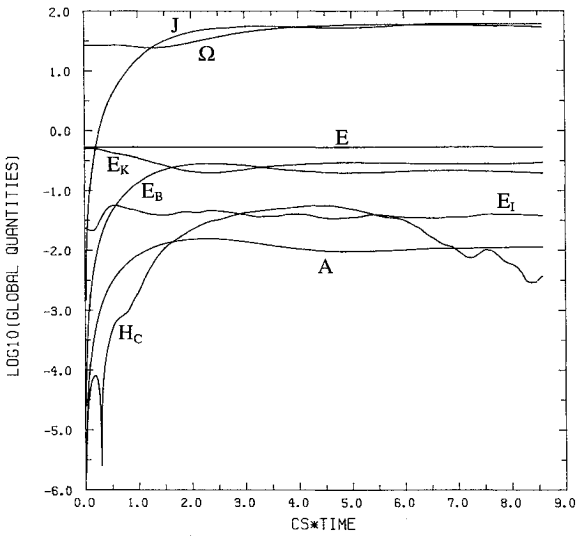

Fig. 3 Run 3: fully spectral, forced, $\nu = \eta = 0.01$, $\beta = 6$, $\gamma = 1.5$, $B_0 = 0.5$.

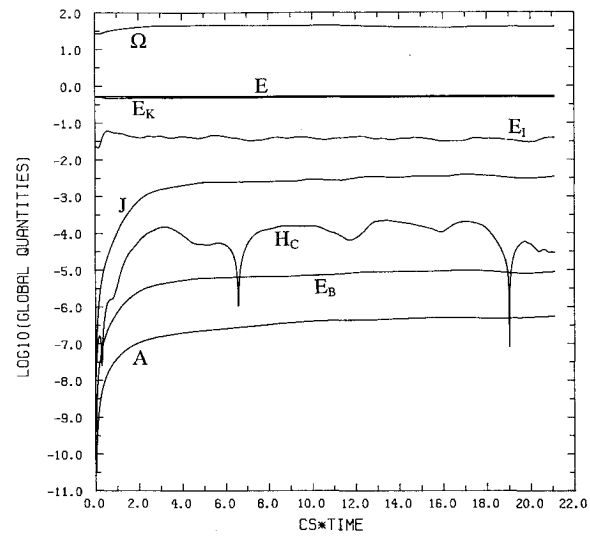

Fig. 5 Run 6: fully spectral, forced, $\nu = \eta = 0.01$, $\beta = 6$, $\gamma = 1.5$, $B_0 = 0.001$.

tion of our code was used. The result is run 7. The global quantities of run 1 are in Fig. 1, and of Run 7 are in Fig. 4; the energy spectra at the end of Runs 1 and 7 are shown in Figs. 9 and 10, respectively. [All the energy spectra presented here are "isotropically averaged": the modal energies $E(k)$, etc., are averaged over all k having the same $k = |\boldsymbol{k}|$ to produce $E(k)$. These $E(k)$ are then "smoothed" by averaging each with its nearest neighbors to produce the various spectral graphs.] A comparison of the global quantities and spectra of runs 1 and 7 shows that they are essentially identical. We also show the final energy spectra of run 3 in Fig. 8 and the isotropic energy spectra of run 6 in Fig. 11. Runs 4, 5, and 6 were similar to run 3, except that $B_0 = 0.2$, 0.05, and 0.001, respectively, rather than 0.5. The global behavior of Run 6 ($B_0 = 0.001$) is shown in Fig. 5. The behavior of J, E_B, and A for runs 4 and 5 are intermediate between those of Runs 3 and 6. As was noted earlier, the initial value of the turbulent magnetic energy E_B was zero with a nonzero B_0; however, E_B increased reaching a final level, which was greater the higher the value of the mean field B_0. An informative quantity is the ratio of E_B to $B_0^2/2$, the volume averaged mean magnetic field energy. We present this ratio for runs 3 through 6 in Table 2. We also note that the local magnetic energy increased, in small regions, to ratios far greater than the ratio of volume averages

Table 2 Final ratio of E_B to $B_0^2/2$

Run	B_0	$E_B/B_0^2/2$
3	0.5	2
4	0.2	6
5	0.05	16
6	0.001	18

given in Table 2; for example, in run 6, the ratio of local magnetic energy density to $B_0^2/2$ was as high as 420 at $\tau = c_s t = 10.7$ (a plot of magnetic energy density at this time is shown in Fig. 20).

One of the reasons for testing the semispectral method was to use it for cases in which the initial Mach number was relatively large, i. e., cases in which compressional energy was increased. Although the semispectral method behaved well in the range of parameters corresponding to runs 1 through 6 where the sound speed was $c_s = 3$, we ran an additional test for the case where $c_s = 1.2$; the test was to compare runs 8 and 9 with the same positive result as before. Run 10 was then performed; it is similar to run 6, in that they both have $B_0 = 0.001$, but the initial rms Mach number for run 10 was 5/6 compared to 1/3 for run 6. The results, shown in Figs. 6

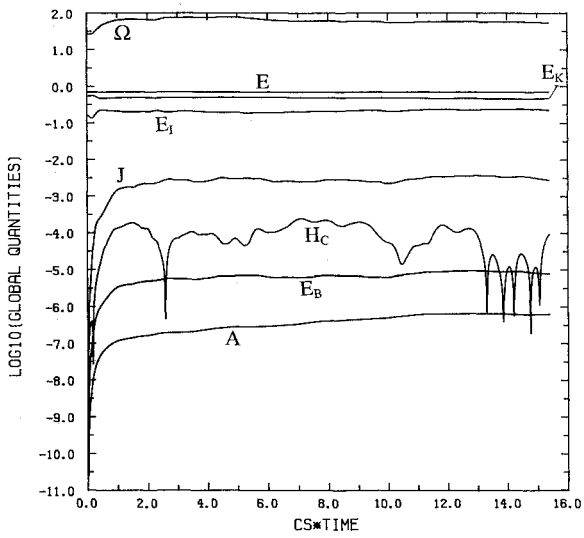

Fig. 6 Run 10: semispectral, forced, $\nu = \eta = 0.01$, $\beta = 1$, $\gamma = 1.44$, $B_0 = 0.001$.

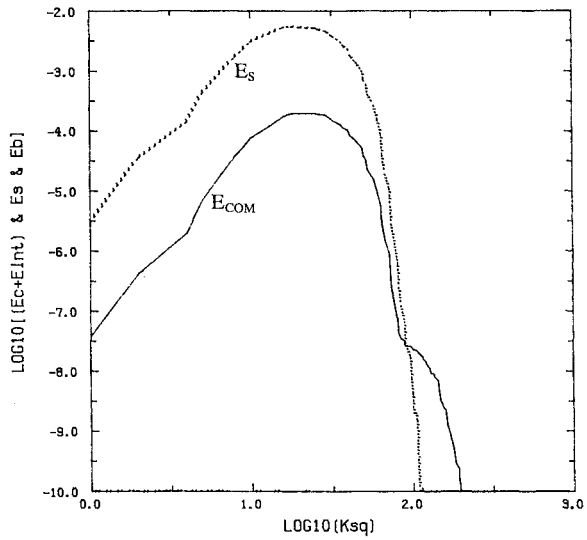

Fig. 7 Initial, isotropically averaged energy spectra for runs 1–7 (initial phases of Fourier coefficients were random); for runs 8–10, E_{com} increased by a factor of 6.9.

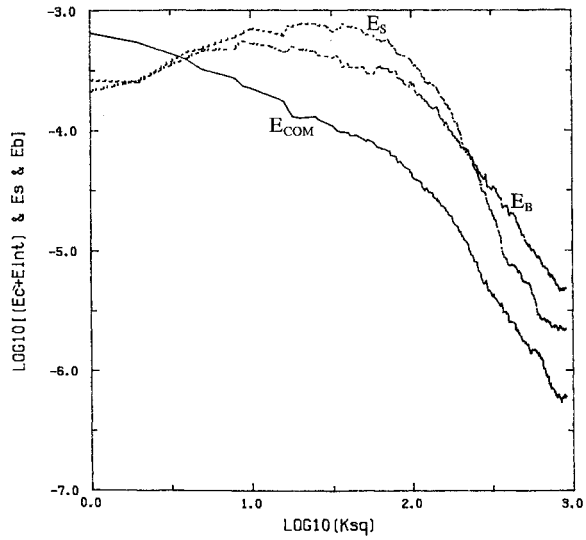

Fig. 8 Isotropically averaged energy spectra for run 3 at $c_s \cdot t = 8.6$.

and 12, indicate that increasing the compressibility did not noticeably affect turbulent magnetic field amplification (although compressional energy obviously increased).

We also present contour plots representative of all the runs in Figs. 13 through 20. Figs. 13, 14, and 15 show density variations. Figure 13 corresponds to run 3, which had $B_0 = 0.5$; this relatively large mean field causes the fluctuations to appear slightly elongated in the direction of the mean field (i.e., horizontally), an anisotropic effect we have pointed out previously for incompressible cases.[15] This elongation tends to produce steeper vertical gradients; this can be seen in comparison with Figs. 14 and 15. In Fig. 14, as in Fig. 13, $c_s = 3$; the steeper gradients in Fig. 13 are then more likely due to the mean field rather than to an increase in compressibility. In Fig. 15, however, $c_s = 1.2$ and $B_0 = 0.001$; therefore the gradients, which are nondirectional, are more likely due to the increase in compressibility.

Another notable feature is the presence of thin current filaments in Fig. 18; these appear as pairs with two thin areas of oppositely directed current pressed close to one another. These small structures manifest themselves again in Fig. 20, a plot of magnetic energy density. In addition to these magnetic structures, there are corresponding fluid structures as evidenced in Figs. 17 and 19; these suggest a strong correlation between small scale (high k) fluid and magnetic phenomena.

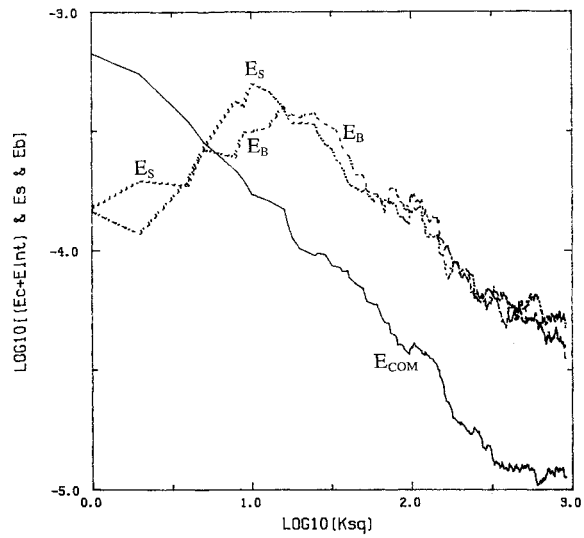

Fig. 9 Isotropically averaged energy spectra for run 1 at $c_s \cdot t = 9.2$.

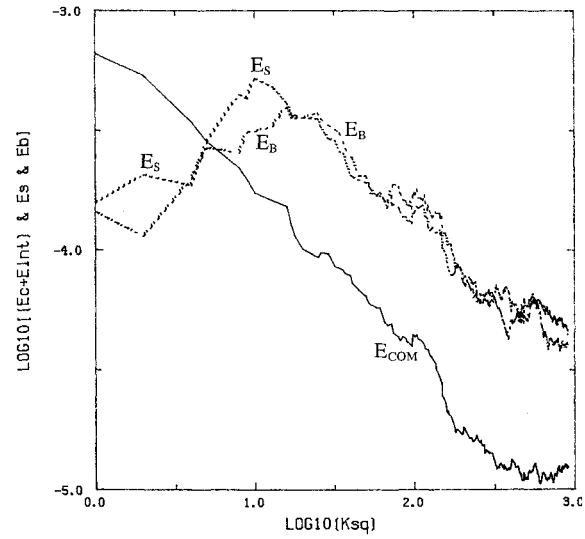

Fig. 10 Isotropically averaged energy spectra for run 7 at $c_s \cdot t = 9.1$ (see Fig. 9).

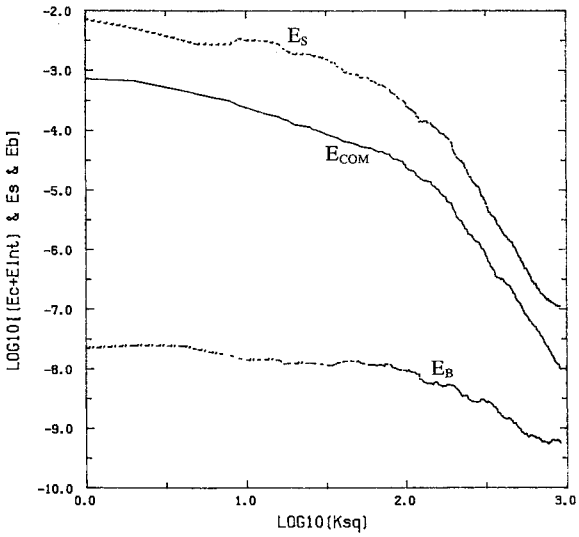

Fig. 11 Isotropically averaged energy spectra for run 6 at $c_s \cdot t = 21.1$.

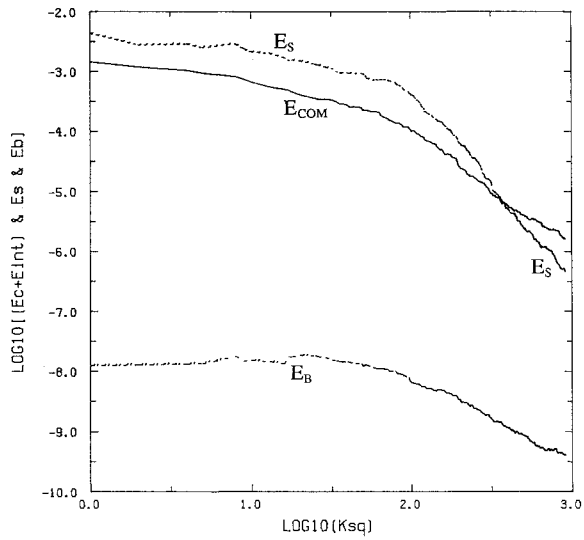

Fig. 12 Isotropically averaged energy spectra for run 10 at $c_s \cdot t = 15.4$.

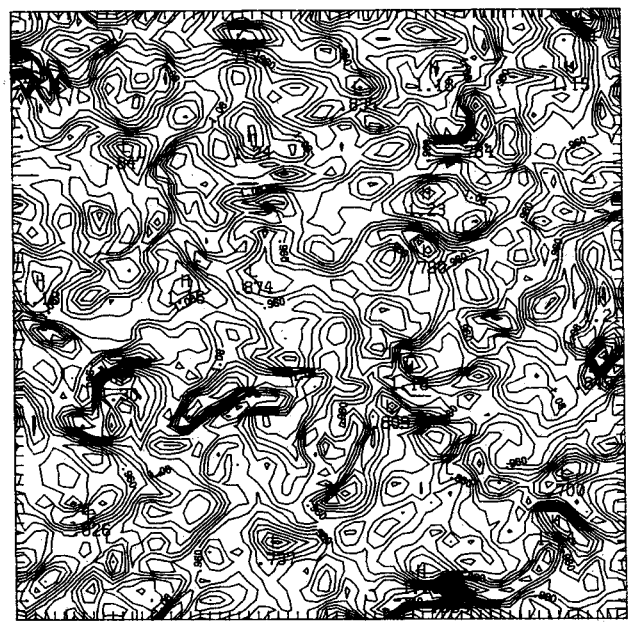

Fig. 13 Density contours for run 3 at $c_s \cdot t = 2.7$; min = 0.86, max = 1.29.

This apparent correlation can be investigated in more quantitative terms by defining the correlation between two spectral functions f and g as

$$\mathrm{cor}_i(f,g) \equiv \frac{\langle f,g\rangle_i}{\sqrt{\langle f,f\rangle_i \langle g,g\rangle_i}}$$

where

$$\langle f,g\rangle_i = \sum_{K_i < k \le K_{i+1}} f(-\boldsymbol{k})\, g(\boldsymbol{k})$$

Here, $i = 1, 2, 3$ corresponds to low, medium, and high spectral ranges, respectively:

$$K_i \equiv \sqrt{\frac{i-1}{3}}\, K_{\max}$$

The above definitions allow us to measure the correlations

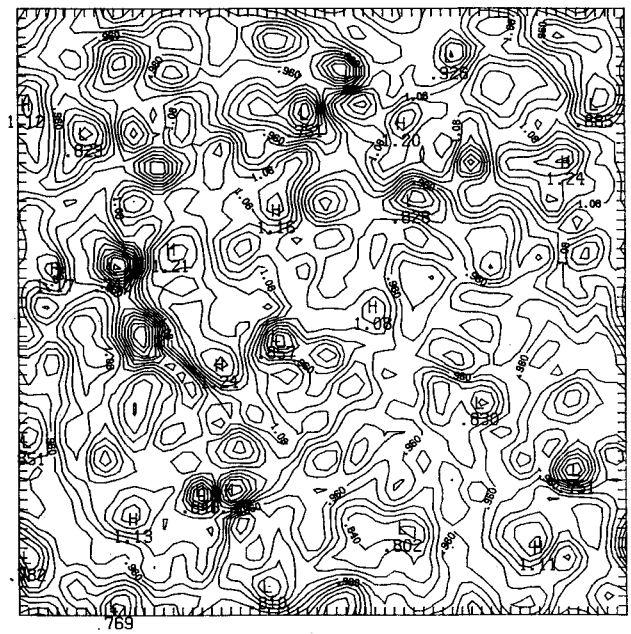

Fig. 14 Density contours for run 6 at $c_s \cdot t = 21.1$; min = 0.72, max = 1.23.

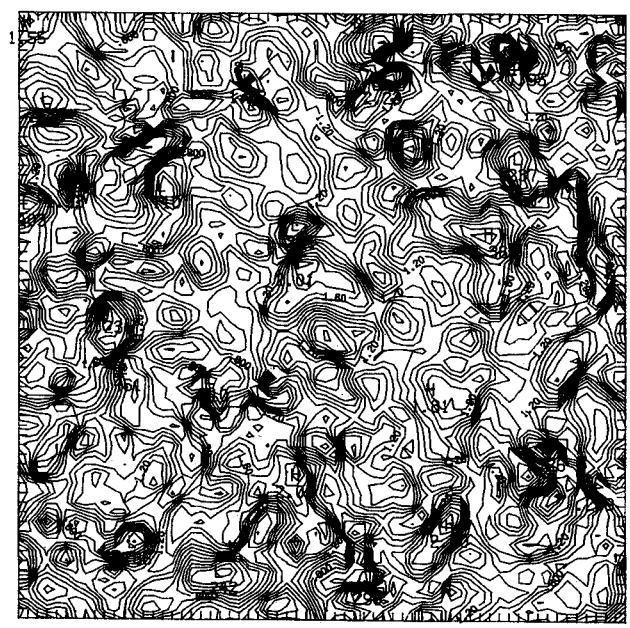

Fig. 15 Density contours for run 10 at $c_s \cdot t = 15.4$; min = 0.10, max = 2.3.

amongst fluctuations in density, velocity, and magnetic field. We do this in Table 3 for the forced, dissipative runs of Table 1. The correlations in Table 3 pertain to the last time steps of the various runs; they are, however, representative of what is happening in the magnetofluid, once any initial transient phenomena have occurred. (Also, in Table 3, $\delta\rho \equiv \rho - \rho_0$.)

As Table 3 shows, there is a moderate correlation between u^2 and b^2 at small k (large spatial scales) for all the forced runs; run 2, an unforced but dissipative run, also had similar behavior. When B_0 is large (as is E_B; see run 3), there seems to be a moderate correlation between density and local magnetic energy fluctuations at high k, which drops, however, as B_0 decreases (runs 4–6). As compressibility increases, there are noticeable effects as a comparison between runs 6 and 10 will show. First, as might be expected, the correlation between density and u^2 fluctuations increases (velocity is high, and density is low and vice versa in compressional motion). Second, the low correlation between density and b^2 at low k grows to a moderate one as compressibility increases. Also,

Table 3 Correlations of Fluctuations

Run	f,g	$\mathrm{cor}_1(f,g)$	$\mathrm{cor}_2(f,g)$	$\mathrm{cor}_3(f,g)$
3	u^2,b^2	0.54	0.09	0.00
	$\delta\rho,b^2$	0.08	0.37	0.49
	$\delta\rho,u^2$	−0.09	−0.10	−0.04
4	u^2,b^2	0.47	0.01	−0.01
	$\delta\rho,b^2$	0.08	0.08	0.22
	$\delta\rho,u^2$	−0.10	−0.19	−0.22
5	u^2,b^2	0.55	−0.04	−0.06
	$\delta\rho,b^2$	0.10	0.04	0.02
	$\delta\rho,u^2$	−0.13	−0.30	−0.41
6	u^2,b^2	0.53	−0.05	−0.06
	$\delta\rho,b^2$	0.12	0.03	0.02
	$\delta\rho,u^2$	−0.12	−0.07	−0.01
10	u^2,b^2	0.50	0.08	0.01
	$\delta\rho,b^2$	0.45	−0.01	−0.01
	$\delta\rho,u^2$	0.24	−0.44	−0.62

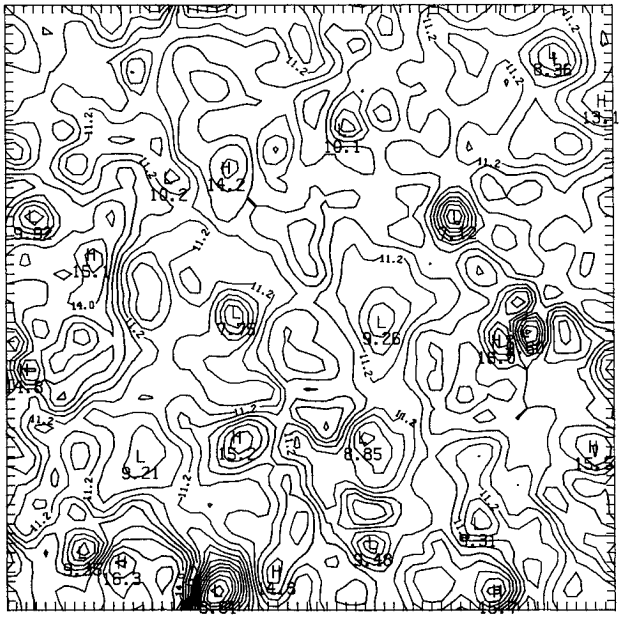

Fig. 16 Pressure contours for run 6 at $c_s \cdot t = 10.7$; min = 3.5, max = 18.1.

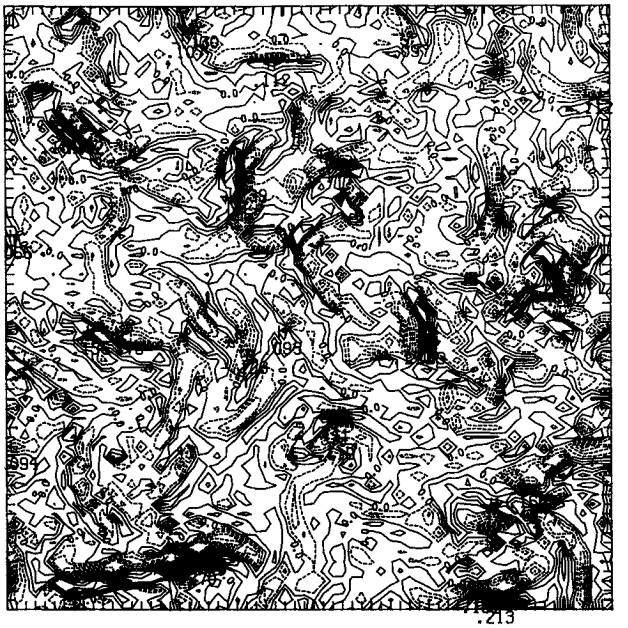

Fig. 18 Current contours for run 6 at $c_s \cdot t = 10.7$; min = −0.24, max = 2.4.

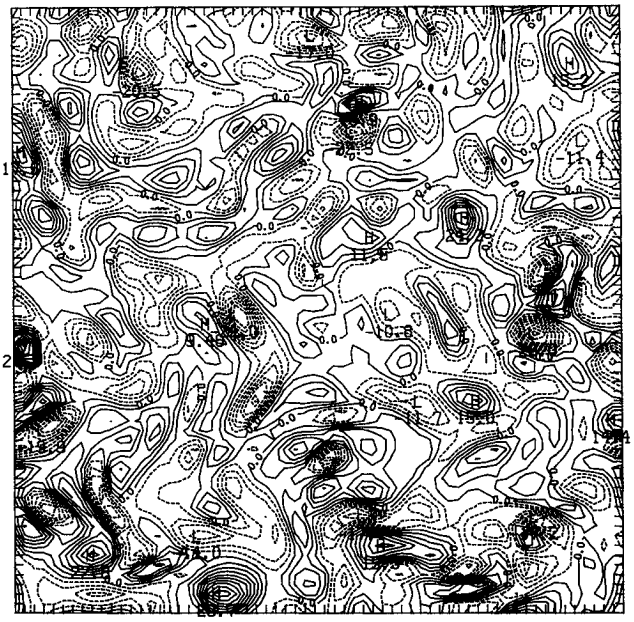

Fig. 17 Vorticity contours for run 6 at $c_s \cdot t = 10.7$; min = −24, max = 27.

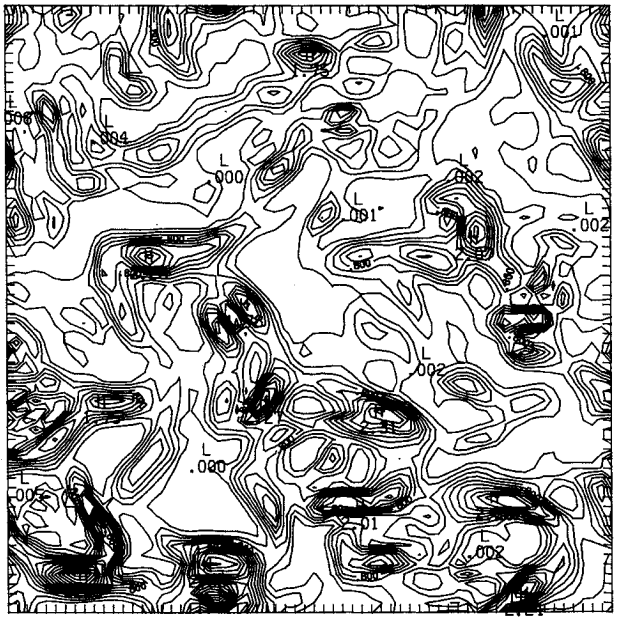

Fig. 19 Kinetic energy density for run 6 at $c_s \cdot t = 10.7$; min = 0.0, max = 3.2.

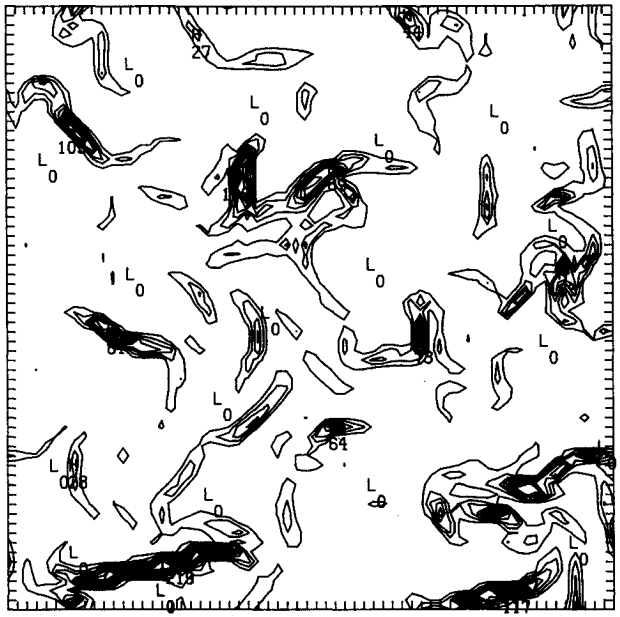

Fig. 20 Magnetic energy density for run 6 at $c_s \cdot t = 10.7$; min = 0.0, max = 2.1×10^{-4}

when there is no forcing (run 2, not shown in Table 2), the correlation between density and b^2 at high k starts off very strong (>0.85) but falls off quickly as the run progresses; this is very similar to a previous $\beta\gamma = 10$ run (run A in Ref. 5; here, run 2 has $\beta\gamma = 9$). Finally, there is a somewhat anomalous behavior in the correlation between density and u^2 in the case of intermediate B_0 (run 5).

In order to distinguish different physical regimes, we note that run 3 has parameters which make it correspond qualitatively to MHD turbulence in the solar wind, and Runs 6 and 10 correspond to MHD turbulence, which may be encountered in the plasma sheath around a hypersonic reentry vehicle. For example, at an altitude of 80 km, with a geomagnetic field of about 0.5 gauss, and a velocity of 10 km/sec, run 6 tells us that the turbulent magnetic field may have rms fluctuations of about 2 gauss and local values of about $\pm$ 10 gauss; whereas the density fluctuations will have an rms value of 10% and a local value of -28% to $+23\%$. In this same situation, run 10 gives us similar magnetic statistics but density fluctuations, which have an rms value of 60% and a local value of -90% to $+130\%$ (but the isentropic, polytropic equation of state, of course, cannot be expected accurately to represent such large density variations).

Conclusion

The principal results from this numerical study are 1) that the presence of a mean magnetic field, even though small, gives rise to significant magnetic field amplification. In fact, when the initial turbulent magnetic field is negligible compared to B_0, the final E_B may be an order of magnitude larger than $B_0^2/2$ (though E_B is still very small compared to E_K). This is suggestive of the classical kinematic dynamo in which a large amount of mechanical energy drives the magnetic field without the magnetic field ever growing large enough to significantly affect the kinetic fluid motions (except, perhaps, in a few isolated local areas); 2) almost tripling the initial Mach number does not appear to have any significant effect on amplification processes; 3) even though the correlation between small scale density and magnetic activity is strong in the initial phase of decaying turbulence (run 2 here and other runs in Refs. 1 and 5), it is at most moderate in forced MHD turbulence (due, probably, to the nature of the random forcing where there was an average equipartition between injected compressional and solenoidal kinetic energy).

The grid size (64×64) that we utilized was suitable for examining the number of cases we did. However, in order to explore fully the small scales at which magnetic effects may be large (even though the total magnetic energy is very small), we need to run at larger grid sizes. Also, the highest Mach number runs need, for better fidelity, a temperature evolution equation rather than the isentropic, polytropic equation of state. These are both planned continuations of our research.

References

[1]Shebalin, J. V., and Montgomery, D., "International Workshop on the Physics of Compressible Turbulent Mixing," Princeton, NJ, Oct. 1988.

[2]Orszag, S. A., *Stud. Appl. Math.*, Vol. 50, 1971, p. 293.

[3]Patterson, G. S., and Orszag, S. A., *Phys. Fluids*, Vol. 14, 1971, p. 2538.

[4]Moffat, H. K., *Magnetic Field Generation Electrically Conducting Fluids*, Cambridge Univ. Press, London, 1978.

[5]Tidman, D. A., and Shanny, R. A., *Phys. Fluids*, Vol. 17, 1974, pp. 1207–1210; also, J. Sheffield, *Plasma Scattering of Electromagnetic Radiation*, Sec. 10.5, Academic Press, NY, 1975.

[6]Shebalin, J. V., and Montgomery, D., *J. Plasma Phys.*, Vol. 39, 1988, p. 339.

[7]Montgomery, D., Brown, M. R., and Matthaeus, W. H., *J. Geophys. Res.*, Vol. 92, 1987, p. 282.

[8]Armstrong, J. W., Cordes, J. M., and Rickett, B. J., *Nature*, Vol. 291, 1981, p. 561.

[9]Lighthill, M. J., *Proceedings of the Royal Society of London, Series A*, Vol. 211, 1952, p. 564.

[10]Dresvin, S. V., ed., *Physics and Technology of Low Temperature Plasmas*, Iowa State Univ. Press, Ames, IA, 1977, Chap. 2.

[11]Braginskii, S. I., "Transport processes in a plasma," *Reviews of Plasma Physics*, Vol. 1, edited by M. A. Leontovich, Consultants Bureau, NY, 1965.

[12]Passot, T., and Pouquet, A., *Journal of Fluid Mechanics*, Vol. 181, 1987, p. 441.

[13]Landau, L. D., and Lifshitz, E. M., *Fluid Mechanics*, 2nd ed., Sec. 33, 1987.

[14]Kraichnan, R. H., and Montgomery, D., *Rep. Prog. Phys*, Vol. 43, 1980, p. 547.

[15]Shebalin, J. V., Matthaeus, W. H., and Montgomery, D., *J. Plasma Phys.*, Vol. 29, 1983, p. 525.